Check for updates

Advanced Intelligent Systems

ADVANCED INTELLIGENT SYSTEMS Open Access

www.advintellsyst.com

RESEARCH ARTICLE OPEN ACCESS

Topological Dielectric Fiber Networks for Self-Powered Teleperception

Yan Du[1,2] | Zhiwei Zhang[3,4] | Cong Li[1,2] | Zihan Wang[1,2] | Jiaxin Guo[1,2] | Zhong Lin Wang[1] | Wei Di[1,5]

[1]Beijing Institute of Nanoenergy and Nanosystems, Chinese Academy of Sciences, Beijing, China | [2]School of Nanoscience and Engineering, University of Chinese Academy of Sciences, Beijing, China | [3]Beijing Huairou Laboratory, Beijing, China | [4]Institute of Thermal Energy Technology and Safety, Karlsruhe Institute of Technology, Karlsruhe, Germany | [5]Centre for Photonic Devices and Sensors, University of Cambridge, Cambridge, UK

Correspondence: Wei Di (weidi@binn.cas.cn)

Received: 12 July 2026 | **Revised:** 24 September 2026 | **Accepted:** 28 September 2026

Keywords: human–machine interaction | teleperception | topological dielectric fiber networks

ABSTRACT

Noncontact sensing is indispensable for intelligent human–machine interaction (HMI), autonomous robotics, and distributed Internet of Things (IoTs). However, the sensing range of existing triboelectric sensors remains fundamentally constrained because dense dielectric architectures limit charge trapping and dielectric polarization. Here, we develop a self-powered triboelectric teleperception sensor (TTS) based on an electrospun poly(vinylidene fluoride)/barium titanate (PVDF/BTO) topological dielectric fiber network. COMSOL simulations, together with experimental characterizations, reveal that the three-dimensional porous topology synergistically enhances charge trapping, electrostatic confinement, and dielectric polarization, while BTO nanoparticles further amplify the interfacial electrostatic field through enhanced dielectric response. These synergistic effects establish an efficient electrostatic induction mechanism for teleperception. Consequently, the TTS achieves a maximum sensing distance of 1.1 m, enables reliable discrimination of target materials and motion frequencies, and supports remote interaction with a robotic arm. Furthermore, a one-dimensional convolutional neural network (1D-CNN) enables intelligent recognition of approaching, receding, waving, walking, and running behaviors with an accuracy of 91.67%. By engineering dielectric topology to regulate electrostatic field coupling, this work establishes a general design strategy for self-powered teleperception, providing a versatile sensing platform for intelligent robotics, HMI, and next-generation embodied systems.

1 | Introduction

The rapid development of human–machine interaction (HMI), intelligent robotics, wearable electronics, and distributed Internet of Things (IoTs) technologies has placed increasing demands on intelligent sensing systems with capabilities for dynamic motion perception, spatial information acquisition, and target recognition [1–3]. As a critical interface bridging the physical world and intelligent devices, high-performance flexible sensors are expected not only to exhibit high sensitivity, excellent stability, and rapid response, but also to enable noncontact and low-power sensing to satisfy the requirements of long-term operation and intelligent interaction in complex environments [4, 5]. To date, flexible sensors mainly include piezoresistive [6, 7], capacitive [8–10], piezoelectric [11–13], iontronics [14–16], and triboelectric types [17–20], all of which rely on mechanical stimuli to convert physical signals into electrical outputs. However, most existing sensors still operate in a contact-based mode, requiring direct physical contact or periodic mechanical stimulation between the target and the sensing interface. Prolonged operation inevitably causes repeated compression, friction, and deformation, leading to functional layer wear, microstructural degradation, and interfacial aging, which ultimately result in baseline drift, deteriorated signal stability, and shortened device

Yan Du, Zhiwei Zhang, and Cong Li contributed equally to this work.

This is an open access article under the terms of the Creative Commons Attribution License, which permits use, distribution and reproduction in any medium, provided the original work is properly cited.

© 2026 The Author(s). *Advanced Intelligent Systems* published by Wiley-VCH GmbH.

lifetime. Moreover, contact-based sensing is inherently confined to local interfacial interactions, limiting its spatial perception capability and restricting its application in noninvasive and noncontact motion recognition.

Triboelectric noncontact sensing based on the electrostatic induction effect has emerged as a promising strategy to overcome the intrinsic limitations of conventional contact-based sensors [21–23]. By detecting variations in the surrounding electrostatic field induced by target motion without mechanical contact, this approach fundamentally eliminates performance degradation caused by friction while offering additional advantages of self-powered operation, structural simplicity, and excellent environmental adaptability. Recently, the concept of teleperception has further advanced the development of triboelectric contactless sensing. Different from infrared [24]- or radio-frequency [25]-based remote detection that pursues extremely large physical detection distances, teleperception emphasizes noncontact intention perception and interactive feedback through spatially extended electrostatic field coupling. It aims to capture faint, time-varying electrostatic field fluctuations induced by target motions within near-to-medium spatial scales and translate these electrostatic time-series signals into recognizable motion features for complex dynamic-motion identification and human–machine interactive feedback [26–29]. These requirements place stringent demands on the charge generation, charge retention, electrostatic field coupling, and anti-interference capability of triboelectric materials. Therefore, developing functional materials with reinforced charge-trapping capacity has emerged as a critical prerequisite for teleperception.

Existing triboelectric materials remain fundamentally limited for teleperception because their dense dielectric architectures restrict interfacial charge generation, storage, and transport [30–32]. Conventional triboelectric film fabricated by spin coating [33, 34] or blade casting [35] typically possess compact microstructures with low specific surface areas, limited charge-trapping sites, and inefficient polarization responses, resulting in reduced surface charge densities and weakened electrostatic field coupling. Therefore, developing dielectric architectures capable of enhancing charge trapping, dielectric polarization, and electrostatic field coupling is crucial for achieving teleperception.

Electrospinning offers a powerful route to engineer such architectures by constructing three-dimensional topological dielectric fiber networks with interconnected porous microstructures and exceptionally high specific surface areas [36–38]. Unlike conventional dense film, these topological fiber networks not only enlarge the effective electrostatic sensing interface but also establish continuous pathways for charge trapping, transport, and polarization, thereby strengthening electrostatic field coupling and extending the response to weak external electric fields. Such topological advantages make dielectric fiber networks a promising materials strategy for teleperception [39].

Herein, a self-powered triboelectric teleperception sensor (TTS) is fabricated based on an electrospun poly(vinylidene fluoride)/barium titanate (PVDF/BTO) topological dielectric fiber network. COMSOL finite-element simulations combined with experimental investigations reveal that the porous fibrous topological network synergistically enhances charge storage, confinement, and transport, thereby improving the electrostatic induction efficiency. Compared with a dense PVDF film of identical thickness, the fibrous topological network exhibits significantly enhanced electrostatic responsiveness, while the incorporation of high-dielectric-constant BTO nanoparticles further strengthens the polarization capability and electrostatic field coupling. As a result, the TTS enables accurate discrimination of different target materials and motion frequencies, achieves a maximum sensing distance of 1.1 m, and facilitates remote interaction with a robotic arm. Furthermore, by integrating a one-dimensional convolutional neural network (1D-CNN), intelligent recognition of human behaviors, including approaching, receding, waving, walking, and running, is achieved with an accuracy of 91.67%. This work provides a charge-trapping strategy for teleperception, paving the way for intelligent HMI, service robotics, smart healthcare, and next-generation IoT applications.

2 | Results and Discussion

2.1 | Structure and Working Mechanism of the TTS

The rapid advancement of teleperception technology has overcome the limitations of conventional contact-based sensing and established a new paradigm for noncontact, low-loss intelligent sensing and interaction (Figure 1a). Figure 1b presents the overall three-dimensional structure of the PVDF/BTO-based TTS fabricated in this work. Copper foil (Cu) serves as the conductive electrode, while electrospun PVDF/BTO composite dielectric fiber film function as the dielectric layer. High-dielectric barium titanate nanoparticles were incorporated into the PVDF matrix, and the electrospinning technique was employed to construct porous fibrous networks, thereby providing the material and structural basis for electrostatic induction and charge storage.

The corresponding microscopic morphology is shown in Figure 1c. The electrospinning process generated interconnected and uniform three-dimensional porous fibrous networks. These fibrous networks exhibited a large specific surface area and abundant interfacial pores, providing sufficient charge-trapping sites and enhancing electric-field coupling. The working mechanism of the TTS for teleperception is illustrated in Figure 1d, and its core response originates from the electrostatic induction effect. When external target objects gradually approach the dielectric layer, obvious electric field gradients emerge between the dielectric film and the targets, triggering the redistribution of induced charges on the film surface. Dynamic variations in the interfacial potential difference further drive the directional migration of electrons through the external circuit. Consequently, electrical signals are generated without mechanical contact or interfacial friction, enabling self-powered sensing of dynamic behaviors such as target approaching and receding. To further reveal the evolution of electric fields and charge distribution during TTS operation, COMSOL finite element simulations were performed to analyze the potential distributions under different sensing states, and the simulated results are presented in Figure 1e. The simulation results verified the electrostatic induction-dominated dynamic potential response mechanism and further demonstrated the evolution characteristics of the potential distribution during the dynamic contact-separation

26404567, 0, Downloaded from https://advanced.onlinelibrary.wiley.com/doi/10.1002/aisy.70583, Wiley Online Library on [19/10/2026]. See the Terms and Conditions (https://onlinelibrary.wiley.com/terms-and-conditions) on Wiley Online Library for rules of use; OA articles are governed by the applicable Creative Commons License

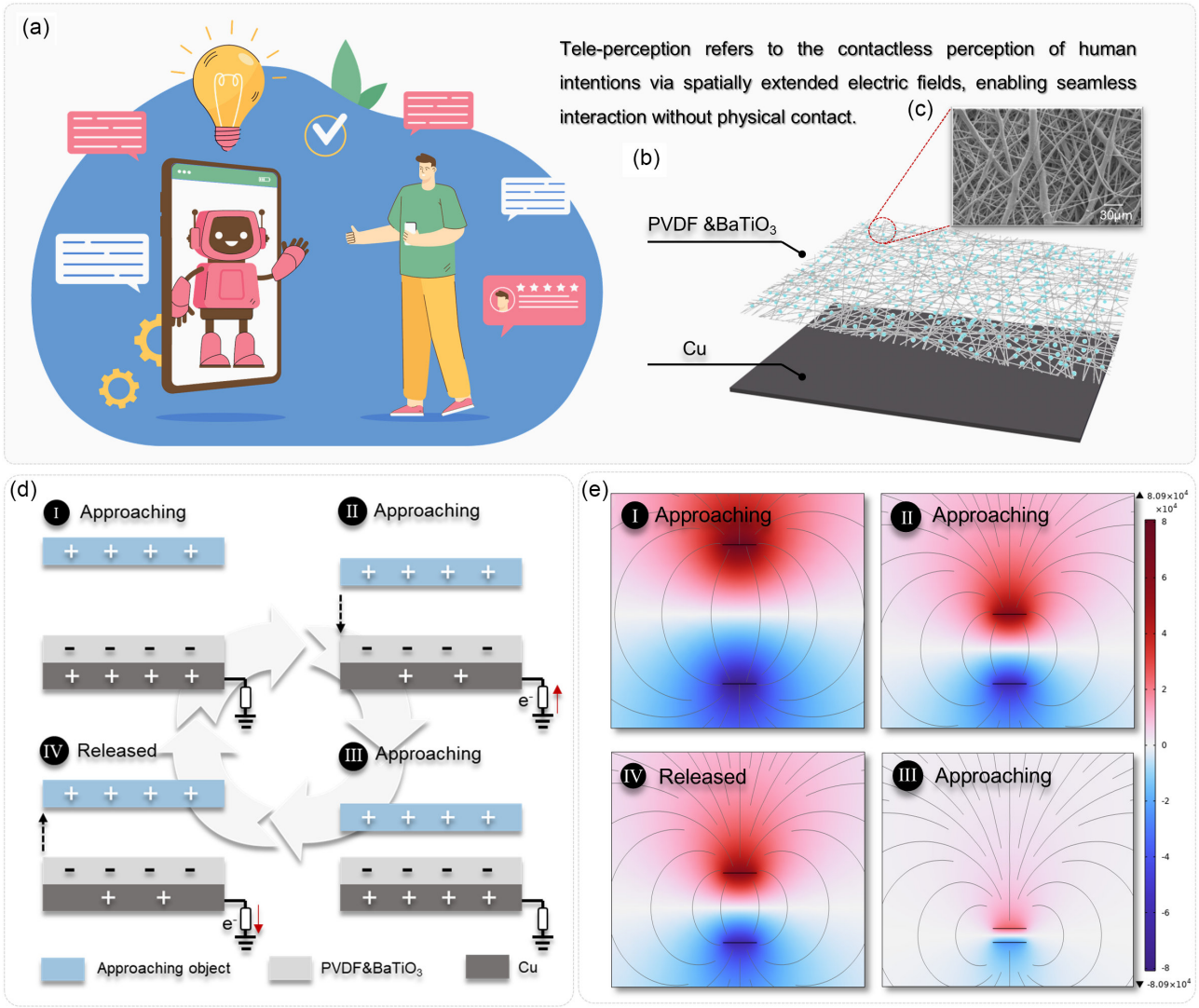


FIGURE 1 | Structure and working mechanism of the TTS. (a) Schematic diagram of the interaction paradigm for teleperception. (b) Three-dimensional structural diagram of the TTS device. (c) SEM morphology of electrospun PVDF/BTO composite fiber film. (d) Working mechanism of the TTS. (e) COMSOL finite element simulation of potential distribution for the TTS.

process, thereby providing a solid physical foundation for the teleperception capability of the TTS.

2.2 | Simulation and Performance of the TTS

To reveal the synergistic enhancement mechanism of microstructural topological regulation and dielectric doping modification on film polarization behavior and electrostatic response characteristics, COMSOL finite element simulations were conducted to systematically investigate the electric field distribution, polarization intensity, and potential output of various film systems, and electrical measurements were carried out to verify their performance. Under the identical film thickness, the simulated polarization electric field distributions of the dense PVDF film, neat electrospun PVDF fiber film, and PVDF/BTO composite fiber film are shown in Figure 2a. Compared with the dense PVDF film, the porous fiber topological structures fabricated via electrospinning effectively optimize the electric field distribution and enhance the interfacial polarization electric field. The incorporation of high-dielectric BTO nanoparticles further amplifies the local electric field and markedly strengthens the polarization effect of the film. The corresponding simulated polarization intensity results are presented in Figure 2b. The internal polarization arrangement of the dense PVDF film is disordered with low polarization efficiency. The electrospun porous structures effectively regularize the polarization orientation and increase the overall polarization intensity, while BTO doping further promotes ordered polarization, greatly improving the polarization uniformity and polarization level of the film.

To determine the optimal BTO doping ratio, we performed systematic potential simulations and electrical output measurements on three types of films: dense PVDF film, neat electrospun PVDF fiber film, and PVDF/BTO composite fiber films with different BTO mass fractions (1, 3, 5, 7, and 9 wt%). Simulated potential distributions (Figure 2c) and measured output voltage curves (Figure 2d) show that PVDF/BTO composite fiber films achieve superior output performance relative to dense PVDF film and neat electrospun PVDF fiber film. Within the composite series,

26404567, 0, Downloaded from https://advanced.onlinelibrary.wiley.com/doi/10.1002/aisy.70583, Wiley Online Library on [19/10/2026]. See the Terms and Conditions (https://onlinelibrary.wiley.com/terms-and-conditions) on Wiley Online Library for rules of use; OA articles are governed by the applicable Creative Commons License

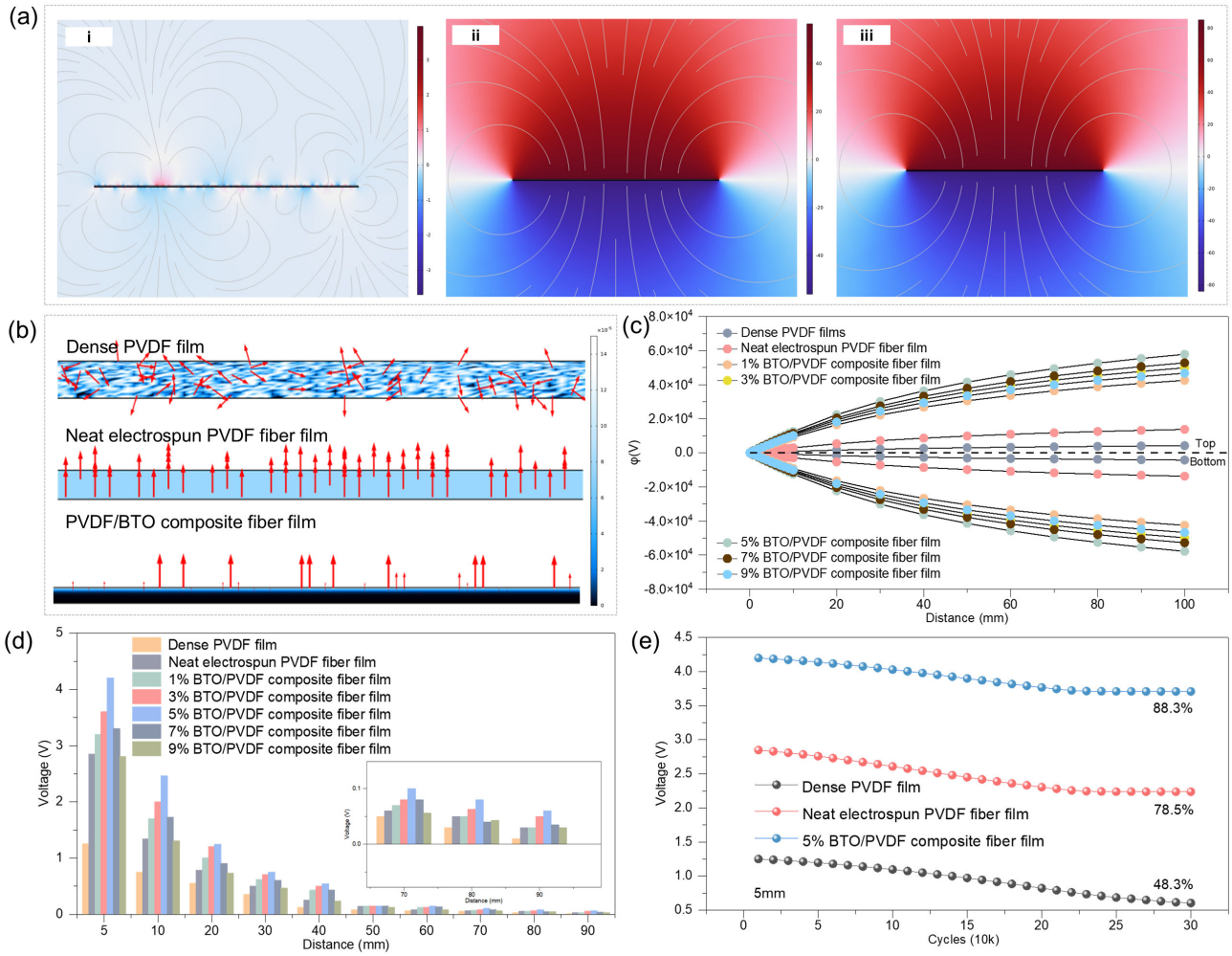


FIGURE 2 | Comparison of polarization characteristics and electrical outputs of film with different structures. (a) Simulated polarization electric field distributions of dense PVDF film, neat electrospun PVDF fiber film, and PVDF/BTO composite fiber film at identical thickness. (b) Corresponding simulated polarization intensity comparison of dense PVDF film, neat electrospun PVDF fiber film, and PVDF/BTO composite fiber film with identical thickness. (c) Simulated potential distributions of dense PVDF film, neat electrospun PVDF fiber film, and PVDF/BTO composite fiber film with various BTO doping ratios (the red arrows indicate the direction of dielectric polarization). (d) Output voltage performance of TTS based on dense PVDF film, neat electrospun PVDF fiber film, and PVDF/BTO composite fiber film with different BTO doping ratios. (e) Cycle stability tests of the TTS based on dense PVDF film, neat electrospun PVDF fiber film, and 5% PVDF/BTO composite fiber film.

sensor output first increases and then decreases with rising BTO loading, and the 5 wt% BTO sample exhibits the strongest electrostatic response and electrical output. Moderate BTO incorporation optimizes charge polarization and electric-field coupling via dielectric enhancement. Low BTO loading provides insufficient dielectric reinforcement, while excessive doping induces nanoparticle agglomeration and extra interfacial defects, hindering charge transport, reducing polarization efficiency, and degrading TTS output. SEM images characterize the micromorphology of these films (Figure S1). BTO nanoparticles disperse uniformly within PVDF fibers at 1 and 3 wt%, while obvious aggregation occurs at 7 and 9 wt%. We further measured the relative permittivity and dielectric loss to verify the dielectric enhancement effect (Figure S2). Relative permittivity rises monotonically with BTO content, accompanied by increased dielectric loss, so the 5 wt% sample achieves the optimal balance between polarization and loss. We also tested the environmental anti-interference performance of TTSs based on dense PVDF film, neat electrospun PVDF fiber film, and 5 wt% PVDF/BTO composite fiber film under different humidity and temperature (Figures S3 and S4). Benefiting from the porous fiber network and BTO-mediated charge trapping, the 5 wt% composite film shows better resistance to signal decay under high humidity and elevated temperature than the other two samples.

To verify the effects of microstructural engineering and dielectric doping on the long-term reliability of the TTS, cyclic stability tests were conducted under the contact-separation mode at 1 Hz with a displacement of 30 mm over 300 000 operating cycles. Devices based on a dense PVDF film, neat electrospun PVDF fiber film, and 5 wt% BTO/PVDF composite fiber film were tested (Figure 2e). The output performance of the three types of TTSs retained 48.3%, 56.14%, and 88.3% of their initial values after 300 000 cycles, respectively. Compared with the dense PVDF film, the electrospun porous fiber network buffers cyclic loads and mitigates structural fatigue, which improves the sensor's resistance to performance degradation. BTO dielectric modification further optimizes interfacial charge storage and charge retention,

26404567, 0, Downloaded from https://advanced.onlinelibrary.wiley.com/doi/10.1002/aisy.70583, Wiley Online Library on [19/10/2026]. See the Terms and Conditions (https://onlinelibrary.wiley.com/terms-and-conditions) on Wiley Online Library for rules of use; OA articles are governed by the applicable Creative Commons License

enhancing the long-term operational stability of the TTS. These results validate that the synergistic strategy combining porous topological structures and dielectric doping improves the long-term stability of the TTS.

2.3 | Teleperception Performance of the TTS

To systematically evaluate the teleperception capacity of the TTS, comprehensive electrical response measurements were performed under diverse conditions, including different target materials, motion frequencies, detection distances, and human dynamic behaviors. Figure 3a presents the voltage response profiles of the TTS toward typical substances including nylon, paper, acrylic, rubber, polytetrafluoroethylene (PTFE), and fluorinated ethylene propylene (FEP) at different distances. The results revealed that the TTS generates distinct and stable electrical signals for materials with different dielectric properties, demonstrating its excellent capability for multi-target discrimination and object recognition. Meanwhile, the TTS exhibits favorable adaptability and stable responses to dynamic excitations over a wide range of motion frequencies (Figure 3b). It maintains reliable signal outputs despite frequency variations, thereby satisfying the continuous sensing requirements of complex dynamic environments.

Human approaching tests confirmed a maximum effective sensing distance of 1.1 m for the TTS (Figure 3c). The time axis in Figure 3c records the real-time signal acquisition during the continuous approaching motion of the human target, and the voltage profile shows the dynamic response of the TTS throughout this process. These results confirm the effectiveness of the synergistic strategy combining porous topological engineering and dielectric modification in enhancing the teleperception capability of the TTS. Furthermore, the TTS recorded unique electrical signal signatures in response to five representative human locomotion modes: approaching, receding, waving, walking, and running (Figure 3d). Marked disparities in signal amplitude and waveform were detected across distinct motion patterns, yielding discriminative signal features that enabled subsequent high-accuracy intelligent classification. To further explore the application potential of the TTS for the HMI, a test platform integrated with a robotic arm was established. As illustrated in Figure 3e, the TTS was attached underneath the robotic arm. When a human gradually approached the robotic arm, the TTS rapidly captured faint electric field variations and produced valid induced signals. These signals triggered the robotic arm's recognition feedback to perform an automatic handshaking interaction (Video S1). This enabled self-powered, noncontact intelligent HMI, demonstrating the strong potential of the TTS for applications in intelligent robots and flexible interactive systems.

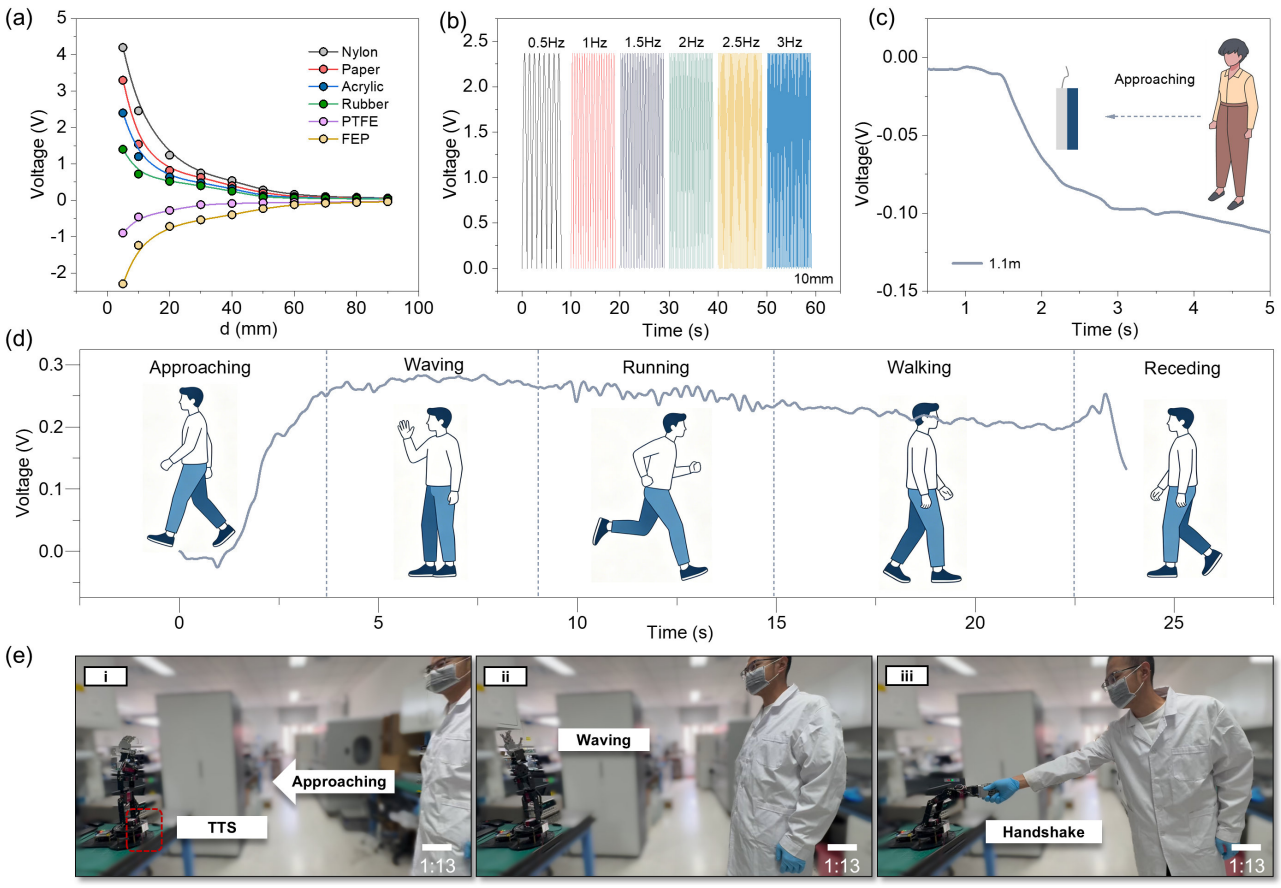


FIGURE 3 | Teleperception performance of the TTS. (a) Output voltages of the TTS toward different materials at various distances. (b) Voltage responses of the TTS under diverse motion frequencies. (c) Test of the maximum effective sensing distance of the TTS under human approaching mode. (d) Response signals of the TTS to typical human dynamic behaviors, including approaching, receding, waving, walking, and running. (e) Remote interactive demonstration of a robotic arm based on the TTS.

26404567, 0, Downloaded from https://advanced.onlinelibrary.wiley.com/doi/10.1002/aisy.70583, Wiley Online Library on [19/10/2026]. See the Terms and Conditions (https://onlinelibrary.wiley.com/terms-and-conditions) on Wiley Online Library for rules of use; OA articles are governed by the applicable Creative Commons License

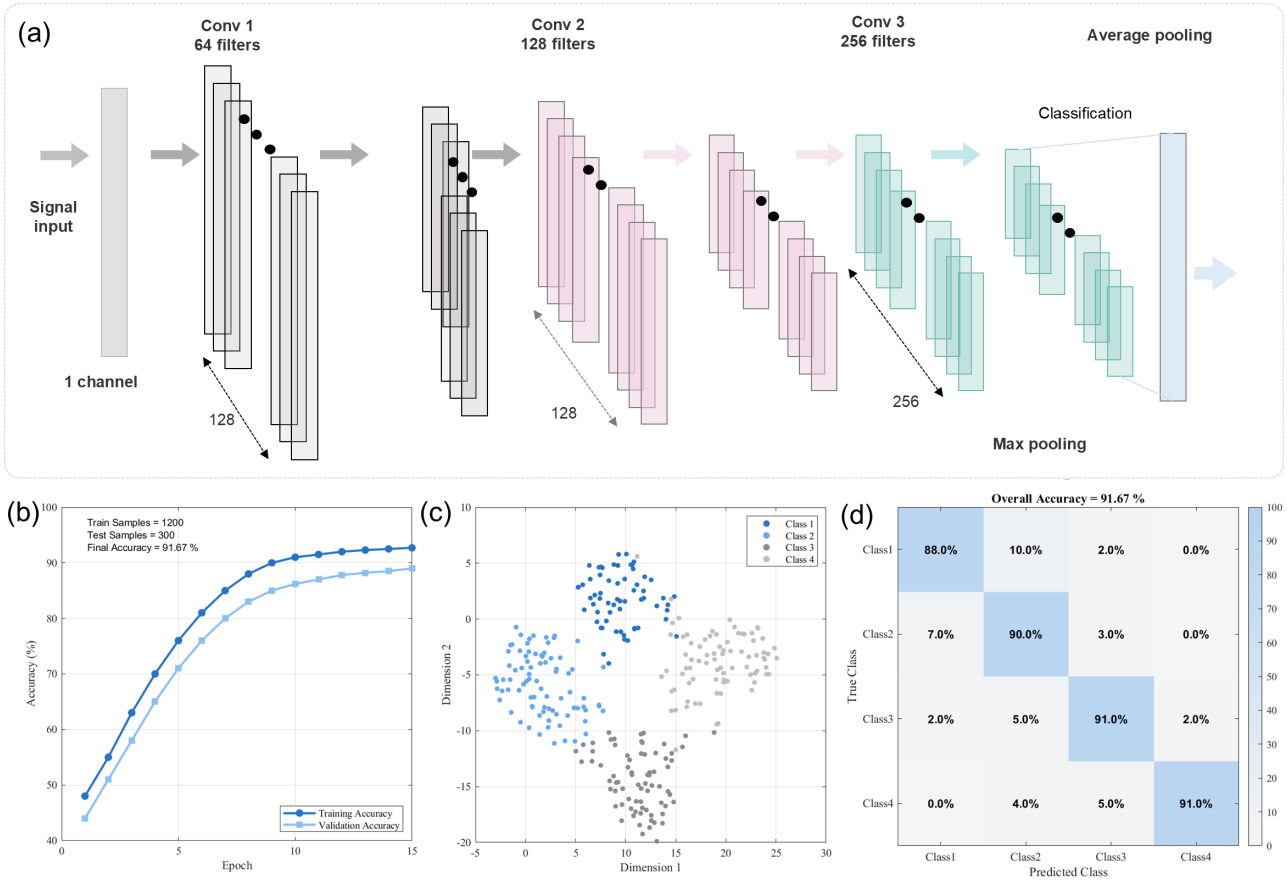


FIGURE 4 | Intelligent recognition of TTS teleperception assisted by 1D-CNN. (a) Overall structural schematic of the 1D-CNN neural network. (b) Iterative convergence curve of model training. (c) Visual scatter plot of human behavior feature clustering. (d) Confusion matrix for the recognition of five types of human dynamic behaviors.

2.4 | Machine Learning-Assisted Teleperception of TTS

To further explore the latent features of the time-series electrical signals acquired by the TTS during teleperception, avoid subjective bias introduced by manual feature extraction, and overcome the limitations of conventional identification methods in terms of accuracy and generalization, a one-dimensional convolutional neural network (1D-CNN) was constructed to enable automatic feature learning and high-accuracy intelligent classification of TTS sensing signals. The overall architecture of the proposed 1D-CNN model is illustrated in Figure 4a. The network takes the original time-series electrical response signals collected by the TTS as the input. It automatically extracts local discriminative features through multiple convolutional layers; performs feature dimensionality reduction, redundant information removal, and background noise suppression via pooling layers; and conducts multidimensional feature fusion and reconstruction through fully connected layers. A precise mapping relationship between teleperception electrical signals and human dynamic behavior attributes is thereby established, enabling the intelligent and refined analysis of self-powered sensing signals.

Five representative human dynamic behaviors, including approaching, receding, waving, walking, and running, were selected as the target classes for model training and intelligent classification. The training convergence curve of the 1D-CNN model is shown in Figure 4b. As the number of training iterations increased, the training loss continuously decreased and eventually converged to a stable value, indicating that the proposed network achieved favorable fitting capability and training stability without obvious overfitting or underfitting. To intuitively evaluate the feature discrimination capability of the model, dimensionality reduction and visualization analyses of the extracted high-dimensional features were performed using clustering scatter plots. As shown in Figure 4c, the feature samples corresponding to the five human behaviors formed well-separated clusters with clear category boundaries, demonstrating that the proposed 1D-CNN model can accurately extract discriminative signal features associated with different human motion patterns. The confusion matrix of the classification results is shown in Figure 4d. The results demonstrated that the 1D-CNN-assisted TTS intelligent sensing system achieved an average recognition accuracy of 91.67% for the five categories of human dynamic behaviors, enabling stable and high-accuracy classification of different human motion patterns. This provides a reliable foundation for intelligent HMI and next-generation self-powered sensing applications.

3 | Conclusion

In summary, we developed a self-powered TTS based on topological dielectric fiber networks, in which electrospun PVDF/$BaTiO_3$

26404567, 0, Downloaded from https://advanced.onlinelibrary.wiley.com/doi/10.1002/aisy.70583, Wiley Online Library on [19/10/2026]. See the Terms and Conditions (https://onlinelibrary.wiley.com/terms-and-conditions) on Wiley Online Library for rules of use; OA articles are governed by the applicable Creative Commons License

composite fibers overcome the intrinsic limitations of conventional dense dielectric film for teleperception. The interconnected three-dimensional fiber topology provides enlarged sensing interfaces, abundant charge-trapping sites, and continuous transport pathways, while $BaTiO_3$-induced dielectric enhancement further strengthens polarization and electrostatic field coupling. Through the synergistic regulation of dielectric topology and polarization characteristics, the optimized network achieves enhanced charge generation, storage, and transport, maintaining 88.3% of its initial output after 300 000 operation cycles. The resulting TTS enables material and motion-frequency discrimination, extends teleperception to a maximum sensing distance of 1.1 m, and supports recognition of diverse human motions, including approaching, receding, waving, walking, and running. Integration with a one-dimensional convolutional neural network further enables adaptive feature extraction and intelligent motion classification with an average accuracy of 91.67%, demonstrating robust perception under complex conditions. The capability of remote robotic handshake interaction highlights its potential for practical HMIs. More broadly, this work establishes topological dielectric fiber networks as a general materials strategy for self-powered teleperception, opening new opportunities for intelligent robotics, smart healthcare, and next-generation autonomous sensing systems.

4 | Experimental Section

4.1 | Materials

PVDF and BTO nanoparticles were used as the raw materials for the preparation of the electrospun composite dielectric film.

4.2 | Fabrication of the TTS

The PVDF/BTO composite solution containing 5 wt% BTO nanoparticles was uniformly dispersed to form the precursor solution. The precursor solution was loaded into a pump-controlled syringe for electrospinning over 4 h. An applied voltage of 15 kV was adopted, the distance between the syringe nozzle and the rotating collector was approximately 10 cm, and the collector rotation speed was set at 1500 rpm to obtain the nanofiber membrane. The as-prepared PVDF/BTO composite dielectric film has a planar area of 3 cm × 3 cm with a fiber-layer thickness of approximately 60 μm. Cu foil was adhered to the back of the composite film as the conductive electrode to assemble the TTS, yielding a final sensor device with an overall area of 3 cm × 3 cm.

4.3 | Characterizations

Before conducting any sensing tests, the as-prepared TTS was precharged using a high-voltage polarization instrument (Nanjing Entai Electronic Instruments, ET 2673A) to endow the PVDF/BTO dielectric fiber layer with initial surface charges for teleperception. A linear motor (LinMot S01-72/500) was employed to precisely control the relative distance and motion state between the target object and the TTS, enabling quantitative and repeatable teleperception tests. The open-circuit voltage signals of the TTS were recorded using a high-precision programmable electrostatic voltmeter (Keithley 6514). For synchronous acquisition and real-time analysis of electrical output characteristics, the Keithley 6514 electrometer was connected to a National Instruments data acquisition card (NI 6346). A customized data acquisition program based on the LabVIEW platform was utilized for automatic signal collection, real-time data processing, and long-term data storage, which guaranteed the accuracy, stability, and reproducibility of all experimental results.

Author Contributions

Yan Du: data curation (lead); investigation (lead); writing – original draft (lead). **Zhiwei Zhang:** Formal analysis (supporting). **Zihan Wang:** validation (supporting). **Jiaxin Guo:** validation (supporting). **Zhong Lin Wang:** supervision (supporting). **Di Wei:** supervision (lead); writing – review and editing (lead).

Acknowledgments

We sincerely acknowledge the financial support from the National Natural Science Foundation of China (Grant No. 22479016).

Funding

This study was supported by the National Natural Science Foundation of China (Grant No. 22479016).

Conflicts of Interest

The authors declare no conflicts of interest.

Data Availability Statement

The data that support the findings of this study are available from the corresponding author upon reasonable request.

References

1. T. Liu, M. Zhang, Z. Li, et al., "Machine Learning-Assisted Wearable Sensing Systems for Speech Recognition and Interaction," *Nature Communications* 16 (2025): 2363.

2. C. Yao, S. Liu, Z. Liu, et al., "Deep Learning-Enhanced Anti-Noise Triboelectric Acoustic Sensor for Human-Machine Collaboration in Noisy Environments," *Nature Communications* 16 (2025): 4276.

3. I. Lee, H. Shin, H. Cho, J.-G. Choi, G. Wang, and S. Park, "Skin-Conformal Electronics for Intelligent Gesture Recognition," *Nature Reviews Electrical Engineering* 2 (2025): 736–754.

4. F. Wen, Z. Zhang, T. He, and C. Lee, "AI Enabled Sign Language Recognition and VR Space Bidirectional Communication Using Triboelectric Smart Glove," *Nature Communications* 12 (2021): 5378.

5. X. An, S. Luo, H. Zhang, et al., "Autonomous Navigation of Intelligent Microrobotic Swarms in Unknown Environments," *Nature Machine Intelligence* 8 (2026): 955–968.

6. P. G. Steeneken, K. Le Phan, M. J. Goossens, et al., "Piezoresistive Heat Engine and Refrigerator," *Nature Physics* 7 (2011): 354–359.

7. C. So, J. U. Kim, H. Luan, et al., "Epidermal Piezoresistive Structure With Deep Learning-Assisted Data Translation," *Npj Flexible Electronics* 6 (2022): 70.

8. K. H. Cho, J.-H. Lee, S. Yun, et al., "Hyperpacked Piezoelectric-Powered Capacitive Sensor Array for High-Fidelity Vibration Detection," *Nature Sensors* 1 (2026): 73–84.

9. A. Berman, K. Hsiao, S. E. Root, et al., "Additively Manufactured Micro-Lattice Dielectrics for Multiaxial Capacitive Sensors," *Science Advances* 10 (2024): eadq8866.

26404567, 0, Downloaded from https://advanced.onlinelibrary.wiley.com/doi/10.1002/aisy.70583, Wiley Online Library on [19/10/2026]. See the Terms and Conditions (https://onlinelibrary.wiley.com/terms-and-conditions) on Wiley Online Library for rules of use; OA articles are governed by the applicable Creative Commons License

10. X. He, B. Zhang, Q. Liu, et al., "Highly Conductive and Stretchable Nanostructured Ionogels for 3D Printing Capacitive Sensors With Superior Performance," *Nature Communications* 15 (2024): 6431.

11. P.-E. Zhou, J.-G. Li, W.-Y. He, et al., "Real-Time Mapping of High-Degree-of-Freedom and High-Fidelity Gestures Based on Piezoelectric Sensor Clusters," *SmartSys* 1 (2025): e70014.

12. G. Han, Y.-F. Su, R. He, et al., "Real-Time Concrete Strength Monitoring Using Piezoelectric Sensors and Deep Learning," *Nature Communications* 17 (2026): 473.

13. C.-X. Xing, Q.-B. Zhang, Z.-H. Wang, et al., "Soft-Metal Bonding-Enabled Recyclable and Anti-Interference Flexible Multilayer Piezoelectric Sensor for Tractor Tire Strain Monitoring," *Nano Energy* 127 (2024): 109704.

14. Y. Du, Z. L. Wang, D. Chu, G. Amaratunga, and D. Wei, "Iontronics for Adaptive and Flexible Pressure Sensing," *Iontronics* 2 (2026): 13.

15. N. Zhang, Y. He, and L. Wang, "Designing Iontronic Pressure Sensors: A Perspective From Multiscale Mechanics," *Iontronics* 1 (2025): 5.

16. X. Wang, C. Guo, Z. Su, et al., "Flexible Iontronic Pressure Sensing Technology: Advanced Structural Ionic Layer," *Iontronics* 2 (2026): 1.

17. Y. Du, P. Shen, H. Liu, et al., "Conformal Self-Powered Inertial Displacement Sensor With Geometric Optimization for In Situ Noninvasive Data Acquisition," *Advanced Functional Materials* 34 (2024): 2409602.

18. X. Li, Y. Guo, C. Li, et al., "Recent Advances in Cutaneous Haptic Interfaces: A Review," *SmartSys* 2 (2026): e70018.

19. X. Lu, H. Tan, H. Zhang, et al., "Triboelectric Sensor Gloves for Real-Time Behavior Identification and Takeover Time Adjustment in Conditionally Automated Vehicles," *Nature Communications* 16 (2025): 1080.

20. Y. Du, D. Chu, G. Amaratunga, and D. Wei, "Triboelectric Tactile Sensors for Intelligent Systems," *SmartSys* 2 (2026): e70023.

21. F. Yin, Y. Guo, Z. Qiu, et al., "Hybrid Electronic Skin Combining Triboelectric Nanogenerator and Humidity Sensor for Contact and Non-Contact Sensing," *Nano Energy* 101 (2022): 107541.

22. W. Yin, Y. Xie, J. Long, et al., "A Self-Power-Transmission and Non-Contact-Reception Keyboard Based on a Novel Resonant Triboelectric Nanogenerator (R-TENG)," *Nano Energy* 50 (2018): 16–24.

23. X. Fu, X. Pan, Y. Liu, et al., "Non-Contact Triboelectric Nanogenerator," *Advanced Functional Materials* 33 (2023): 2306749.

24. T. Xu, F. Zhong, P. Wang, et al., "Van der Waals Mid-Wavelength Infrared Detector Linear Array for Room Temperature Passive Imaging," *Science Advances* 10 (2024): eadn0560.

25. H. Zhou, M. Zhou, M. Xiang, et al., "Heterogeneous Integration of Ultrawide Bandgap Semiconductors for Radio Frequency Power Devices," *Science Advances* 11 (2025): eadw6167.

26. Y. Du, P. Shen, H. Liu, et al., "Multi-Receptor Skin With Highly Sensitive Tele-Perception Somatosensory," *Science Advances* 10 (2024): eadp8681.

27. Y. Du, P. Shen, H. Liu, et al., "Meta-Structured Electret Heterointerface for Resilient and Adaptive Tele-Perception in Embodied Intelligence," *Matter* 8 (2025): 102363.

28. Y. Du, Z. Zhang, Z. L. Wang, and D. Wei, "Omnidirectional Tele-Perception Enabled by Nano-Architectured Electret Skin," *iScience* 29 (2026): 114584.

29. J. Guo, Y. Du, Z. Wang, and D. Wei, "A Paradigm Shift From Traditional Non-Contact Sensors to Tele-Perception," *Journal of Materials Chemistry A* 13 (2025): 8939–8967.

30. Y. Du, Z. Wang, and D. Wei, "Advancing Tele-Perception: A Paradigm Shift From Traditional Non-Contact Sensing to Adaptive Embodied Artificial Intelligence Systems," *Science Bulletin* 70 (2025): 1375–1379.

31. J. Wang, S. Xu, and C. Hu, "Charge Generation and Enhancement of Key Components of Triboelectric Nanogenerators: A Review," *Advanced Materials* 36 (2024): 2409833.

32. Z. Meng, T. Zhang, C. Zhang, Y. Shang, Q. Lei, and Q. Chi, "Advances in Polymer Dielectrics With High Energy Storage Performance by Designing Electric Charge Trap Structures," *Advanced Materials* 36 (2024): 2310272.

33. M. V. Kelso, N. K. Mahenderkar, Q. Chen, J. Z. Tubbesing, and J. A. Switzer, "Spin Coating Epitaxial Films," *Science* 364 (2019): 166–169.

34. H. Min, N. Wang, N. Chen, et al., "Spin Coating Epitaxial Heterodimensional Tin Perovskites for Light-Emitting Diodes," *Nature Nanotechnology* 19 (2024): 632–637.

35. X. Yang, Y. Zhu, S. Yan, H. Hu, C. Chen, and J. Tang, "Blade-Coating Perovskites for Tandem Devices: Liquid Mechanism, Film Formation, and Performance," *Solar RRL* 9 (2025): 2500149.

36. X. Cheng, Y.-T. Liu, Y. Si, J. Yu, and B. Ding, "Direct Synthesis of Highly Stretchable Ceramic Nanofibrous Aerogels via 3D Reaction Electrospinning," *Nature Communications* 13 (2022): 2637.

37. X. Cheng, T. Li, L. Yan, et al., "Biodegradable Electrospinning Superhydrophilic Nanofiber Membranes for Ultrafast Oil-Water Separation," *Science Advances* 9 (2023): eadh8195.

38. T. Li, Y. Yuan, L. Gu, et al., "Ultrastable Piezoelectric Biomaterial Nanofibers and Fabrics as an Implantable and Conformal Electromechanical Sensor Patch," *Science Advances* 10 (2024): eadn8706.

39. G. Du, J. Wang, Y. Liu, et al., "Fabrication of Advanced Cellulosic Triboelectric Materials via Dielectric Modulation," *Advanced Science* 10 (2023): 2206243.

Supporting Information

Additional supporting information can be found online in the Supporting Information section.

26404567, 0, Downloaded from https://advanced.onlinelibrary.wiley.com/doi/10.1002/aisy.70583, Wiley Online Library on [19/10/2026]. See the Terms and Conditions (https://onlinelibrary.wiley.com/terms-and-conditions) on Wiley Online Library for rules of use; OA articles are governed by the applicable Creative Commons License